

WO₃ Modified Graphene Supported Pt Electrocatalysts with Enhanced Performance for Oxygen Reduction Reaction

Yanxian Jin^{}, Deman Han, Wenping Jia, Fang Li, Xiaoying Chen, Guobo Huang, Dai Zhang*

School of Pharmaceutical and Chemical Engineering, Taizhou University, Taizhou 318000, China

*E-mail: snowflakej@163.com

Received: 11 April 2017 / Accepted: 22 April 2017 / Published: 12 June 2017

To improve performance of Pt catalyst, the unique Pt/WO₃-G catalysts for oxygen reduction reaction (ORR) are prepared, in which WO₃ modified graphene (WO₃-G) is adopted as a carrier. According to XRD experiment results, Pt/WO₃-G catalysts are primarily composed of Pt nanoparticles, monoclinic WO₃ and graphene. The TEM and high resolution TEM analysis indicate that Pt/WO₃-G catalyst with the coexistence of Pt particles and WO₃ has narrower distribution of Pt particles with average particle size of 3.9 nm. As expected, The Pt/WO₃-G catalysts reveal better electrocatalytic activity with higher current densities, lower overpotential and faster kinetics process compared to the Pt/G catalyst. The enhancement of ORR activity on Pt/WO₃-G electrocatalyst is probably attributed to the synergistic effect between Pt and WO₃ nanoparticles. Specifically, the interaction between Pt and WO₃ can increase the dispersion of Pt nanoparticles, accelerate the protonation of the O₂ molecule and decrease the adsorption strength of oxygenated species.

Keywords: Oxygen Reduction Reaction; Graphene, Pt Electrocatalysts

1. INTRODUCTION

The oxygen reduction reaction (ORR) is one of the most important electrical catalytic reaction [1-4]. At present, the popular cathode catalysts for fuel cells are Pt/C catalysts or Pt-based catalysts [4], which exhibit the superior catalytic activity for ORR. However, the high cost and limited source of Pt, as well as poor corrosion of carbon carrier restricted its application. In addition, the high overpotential and sluggish oxygen reduction kinetics remain the major problems for oxygen reduction process [2-3]. An effective method to enhance the performance of Pt catalyst is to develop new type of catalyst carrier, which improve the distribution of Pt and the microstructure of the catalyst [5]. Carbon materials, such as carbon black, carbon fiber, carbon microspheres and carbon nanotubes [6] are the widely used as carriers of ORR electrocatalysts due to their good electrical conduction ability and large

specific surface area. Compared with other carbon materials, as a new type of two-dimensional carbon material, graphene has larger specific surface area ($2630 \text{ m}^2 \cdot \text{g}^{-1}$), better electrical conduction (about $2 \times 10^5 \text{ cm}^2 \cdot \text{V}^{-1} \cdot \text{s}^{-1}$) [7-8], and special mechanics, quantum, and electrical properties, which has been recognized as more promising material for the fuel cell catalyst carrier. The catalysts with graphene as a support for Pt nanoparticles have been demonstrated to enhance activity and stability for ORR. For instance, Lin, etc. [9] reported that the graphene load Pt catalysts, which exhibited more excellent catalytic properties and better stability than Pt/C catalyst. Liu [10] used functionalized graphene as the carrier to load Pt catalyst, and the results showed that the catalytic performance for ORR and its stability is evidently improved in respect to the commercial Pt/C catalyst. In addition, Jing-hong li group [11] reported that Pt/Graphene catalyst shows excellent catalytic performance for methanol oxidation. It proved that the graphene as a carrier for fuel cell electrocatalysts has obvious advantage.

Another effective method to improve the performance of Pt catalyst is to add transition metal oxides [12-13]. The metal oxides have strong interaction with Pt metal, which can modify the electronic structure and produce synergistic catalytic effect. As a transition metal oxide, tungsten oxide has many stable oxidation states and widely applied in the field of chemical and electrochemical [14-16]. Among them, hexavalent tungsten oxide WO_3 is (the) most stable. Savadogo etc. [17] reported the Pt/ WO_3 catalysts demonstrated enhanced catalytic properties including the greatly improved corrosion resistance for ORR in acidic solution compared to the commercial Pt/C catalyst. Liu and his partners' [14] research also proved that the Pt/ WO_3 catalysts significantly improved catalytic activity and electron transfer ability for ORR in acid medium in comparison with traditional Pt/C catalysts [18-20]. Besides the excellent performance for ORR [18-20], Pt/ WO_3 catalysts also received superior catalytic activity for hydrogen oxidation [21], formic acid oxidation and methanol oxidation [22]. It is obvious that the WO_3 can enhance the catalytic performance of metal Pt. However, the poor conductivity and low specific surface area of WO_3 limits the application in fuel cells.

Taking into consideration the high electrical conductivity and high specific surface area of graphene and synergistic catalytic effects of WO_3 , we design the WO_3 -modified graphene (WO_3 -G) as the carrier to support Pt, which can not only promote more interfaces between WO_3 and noble metals, but also enhance the electrical conductivity and corrosion resistance of the catalyst. Herein, WO_3 modified graphene was prepared as a carrier, and subsequent Pt nanoparticles were deposited using potassium borohydride as reducing agent. And a unique Pt/ WO_3 -G catalyst was obtained and studied for ORR. Importantly, the relationship between the catalyst structure and catalytic performance are explored, and kinetic parameters of catalyst research are studied.

2. EXPERIMENTAL PART

2.1. Catalyst preparation

In the first step, the WO_3 /G was prepared. Firstly, 200 mg of GO material were added to an aqueous solution of ammonium tungstate (10 wt.%, 20 wt.% and 30 wt.%, respectively) and mixed ultrasonically for a while until well dispersed. Secondly, the mixture was maintained at $80 \text{ }^\circ\text{C}$ for 8 h

under vigorous agitation. After filtrated, the precipitate was heat treated at 400 °C under Ar atmosphere for 4 h. Finally, the calcined product was washed with excess ethanol and water respectively. The obtained samples were marked as 10% WO₃-G, 20% WO₃-G and 30% WO₃-G.

In the second step, the Pt/WO₃-G catalysts with different content were synthesized (WO₃ content is 10 wt.%, 20 wt.% and 30 wt.%, respectively). Firstly, 80 mg of WO₃/G was added into 50 mL of water and mixed ultrasonically until well dispersed. Secondly, 4.56 mL of 0.01 mol·L⁻¹ H₂PtCl₆ solution was added into the mixture and sonicated for a while. 120 mL of potassium borohydride solution (2.3 mg/mL) was added into the suspension drop by drop. The reaction continued 6 h at 60 °C under N₂ flow. Finally, the slurry was filtered and washed with excess water, and then dried under vacuum at 80°C. The obtained samples were marked as Pt/10%WO₃-G, Pt/20%WO₃-G and Pt/30%WO₃-G. For comparison purpose, Pt/G sample was also prepared by the similar method. The nominal content of Pt in the catalysts was 10 wt.%.

2.2. Catalyst characterization.

Transmission electron microscopy (TEM) and high resolution transmission electronmicroscope (HRTEM) analysis were conducted on the JEOL-2010 microscope wiht the condition of a potential of 200 kV and a current of 103 mA. X-ray diffraction (XRD) was carried out on Philips PW3040/60 X-ray diffractometer, and the Cu K α radiation of wavelength λ is set at 0.15406 nm.

2.3. Electrochemical measurement.

All electrochemical measurements were performed on a CHI 730d electrochemistry workstation at room temperature.

Working electrodes were prepared from a 5 mm diameter RDE glassy carbon disk during ORR activity measurements under an interchangeable RDE system (Pine Instruments). The catalyst powders were mixed with ethanol and 5 wt.% Nafion solution, and then coated on a mirror-polished glassy carbon disk electrode. Saturated calomel electrode (SCE) was selected as the reference electrode, and Pt foil electrode as the counter electrode.

3. RESULTS AND DISCUSSION

3.1. Physicochemical characterization

Figure 1 shows XRD graphs for Pt/WO₃-G with different contents of WO₃ and Pt/G catalysts. As shown, an intense peak at about 10.9 ° is characteristic of C(002) layer of GO. By contrast, a broad peak at about 26° assigned to the C(002) layer of G can be observed on the Pt/G catalyst, suggesting the successful reduction of GO [23]. Otherwise, four peaks at 39.8 °, 46.2 °, 67.5 ° and 81.2 ° correspond to the (111), (200), (220), (311) facets of face-centered cubic (fcc) Pt crystal respectively (JCPDS No.04-0802), indicating Pt particles exist in the form of fcc structure [24-25]. The XRD patterns of

WO₃-G shows the main peaks matching well with the monoclinic WO₃ (space group P21/n) (JCPDS No.43-1035) [26]. Besides the representative peak of graphene, the characteristic peaks of monoclinic WO₃ and fcc Pt are all observed on Pt/WO₃-G catalysts with different contents of WO₃. It can be concluded that Pt/WO₃-G catalysts are mainly composed of Pt nanoparticles, monoclinic WO₃ and graphene.

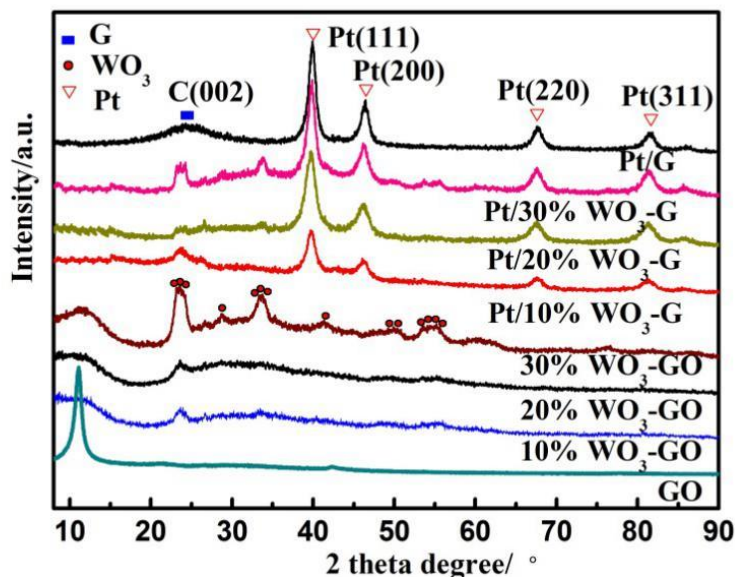


Figure 1. XRD patterns of Pt/WO₃-G with different contents of WO₃ and Pt/G samples

The morphology of catalysts were characterized by tunnel electron microscopy (TEM) analysis. The TEM images of Pt/20%WO₃-G and Pt/G catalysts are shown in Figure 2a,2b. It can be observed that spherical Pt particles relatively evenly distributed on the surface of graphene, but there is a phenomenon of agglomeration on Pt/G. For the Pt/20% WO₃-G catalyst, WO₃ particles with irregular shapes are found on the surface of graphene, and more fine and uniform spherical Pt particles are dispersed on the support. Figure 2c and 2d represent the graphs of Pt particle size distributions. As seen, the Pt particle size distributions on Pt/G catalyst range from 2.5 to 8.5 nm and the average particle size is 4.9 nm. Whereas the Pt/20% WO₃-G catalyst has narrower distribution of Pt particles in a range of 2.0 to 6.5 nm with average particle size of 3.9 nm. This suggests that WO₃ are of benefit to decrease the particle size of Pt nanoparticles, and improve the dispersion of Pt on the carrier.

Figure 4e is the high resolution TEM (HRTEM) image. As shown, the lattice fringe spacing for ~ 0.225 nm is corresponding to the Pt (111) surface. In addition, the spacing of ~ 0.263 nm lattice fringes corresponds to monoclinic WO₃ (220) crystal plane. The spacing values are both consistent with the standard values (JCPDS No. 04-0802 and No. 43-1035). This illustrates the Pt particles and WO₃ coexist in the Pt/20%WO₃-G catalysts, and the results are in accord with the XRD results completely. At the same time, the EDX result of the catalyst confirms that Pt/20%WO₃-G catalyst is mainly composed of C, W, Pt and O elements, as shown in Figure 4f.

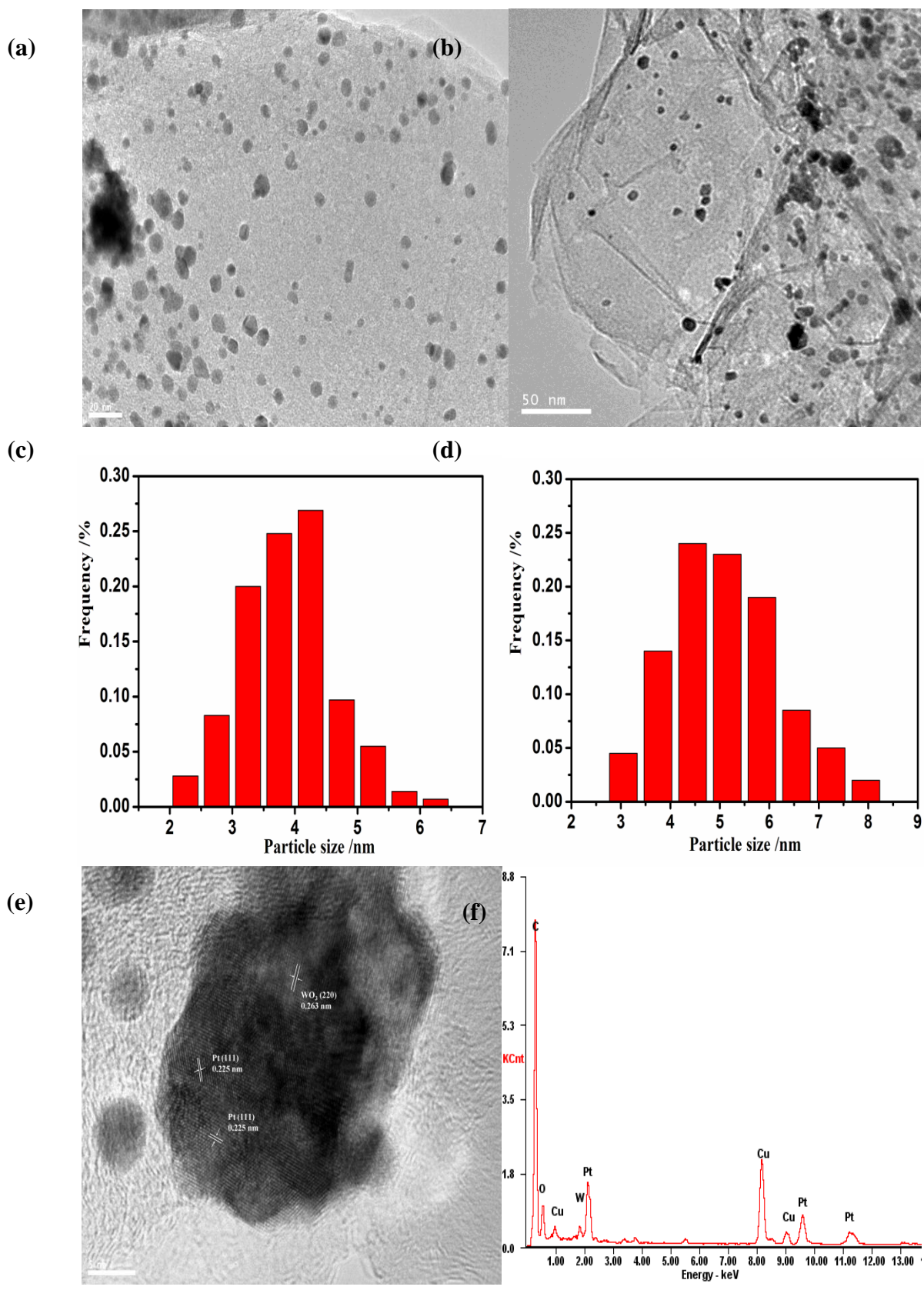


Figure 2. (a) TEM image of Pt/20%WO₃-G; (b) TEM image of Pt/G; (c), (d) Particle size histograms of Pt/20%WO₃-G and Pt/G (e) HRTEM image of Pt/20%WO₃-G (f) EDX image of Pt/20%WO₃-G catalyst

3.2. Electrochemical characterization

The cyclic voltammograms of Pt/G and Pt/WO₃-G catalysts with different content of WO₃ are tested in 0.5 M H₂SO₄ saturated with N₂, which is recorded in Figure 3. As for the Pt/G catalyst, the peaks during -0.2 V - 0.2 V (vs. SCE) in the forward scan are attributable to hydrogen absorption and desorption peaks on Pt. In contrast, the peaks during the interval of -0.2 V - 0.2 V (vs. SCE) on Pt/WO₃-G catalysts increase as the content of WO₃ increase, which suggests the current is ascribed to not only the hydrogen absorption and desorption peaks on Pt, but also the formation of hydrogen tungsten bronzes catalyzed by Pt [27-28].

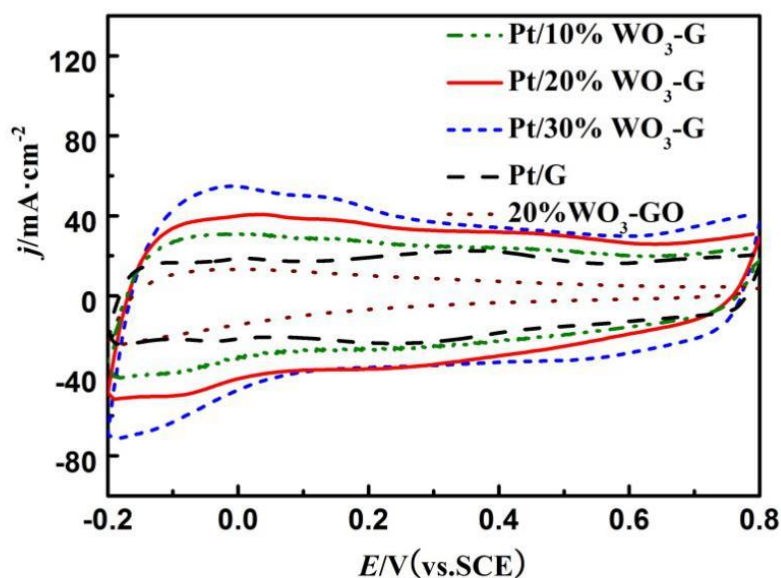


Figure 3. Cyclic voltammograms of Pt/WO₃-G with different contents of WO₃ and Pt/G catalysts electrodes in nitrogen-saturated 0.5 mol·L⁻¹ H₂SO₄ electrolyte with a scan rate of 50 mV/s

The linear sweep voltammetry in O₂-saturated 0.5 mol·L⁻¹ H₂SO₄ with the rotation speed of the working electrodes at 1600 rpm was used to explore the performance to the catalysts, as shown in Figure 4. The oxygen reduction peak at a start of ~ 0.66 V are observed on Pt/G catalyst. Compared with the Pt/G catalyst, the initial potential of oxygen reduction reaction on Pt/WO₃-G catalysts with different content of WO₃ show a positive shift to ~ 0.76 V. The bigger initial reduction potential represents the lower overpotential of oxygen reduction reaction. So, the initial potential of ORR shift about 100 mV positively suggests the overpotential of ORR decrease about 100 mV on Pt/WO₃-G catalysts. At the same time, at the selected potential of 0 V (vs. SCE), the current density of oxygen reduction reaction on all the Pt/WO₃-G catalysts are 6.2 mA·cm⁻², 10.2 mA·cm⁻² and 9.2 mA·cm⁻², which are 1.4, 2.4, and 2.1 times as large as that of Pt/G catalyst (4.3 mA·cm⁻²). The lower overpotential and higher current density suggest that Pt/WO₃-G catalysts have better electrocatalytic activity than Pt/G catalyst, and WO₃ promoted the catalytic performance of Pt for ORR.

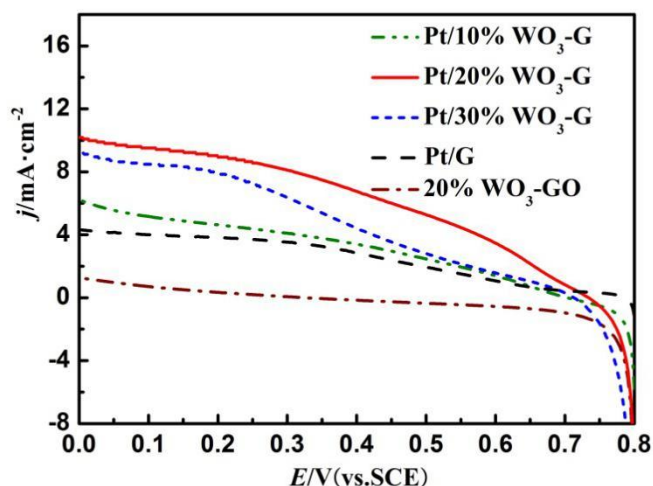


Figure 4. Comparison of the polarization curves for ORR on Pt/G and Pt/ $\text{WO}_3\text{-G}$ with different contents of WO_3 on glass carbon rotating disk electrodes in oxygen-saturated $0.5 \text{ mol}\cdot\text{L}^{-1}$ H_2SO_4 solution with a scan rate of 2 mV/s and a rotation rate of $1600 \text{ r}\cdot\text{min}^{-1}$

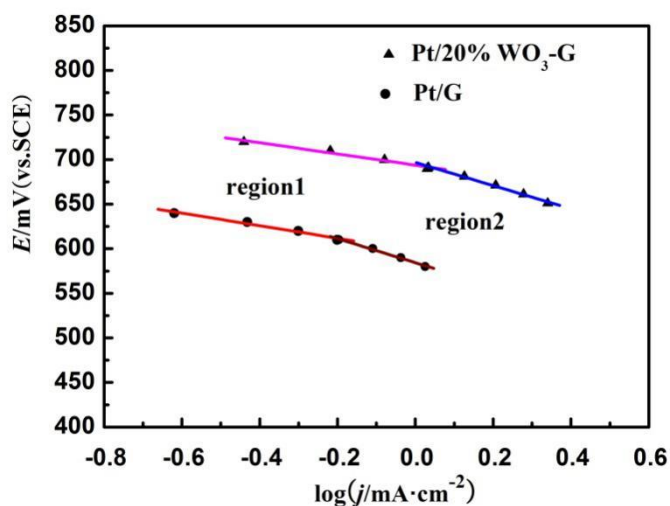
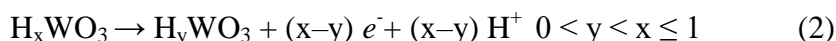
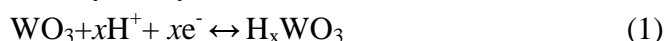


Figure 5. Tafel slopes for ORR on Pt/20% $\text{WO}_3\text{-G}$ and Pt/G electrodes

The Tafel plots were obtained when we replot the data in Figure 4 according to the Tafel equation, which is shown in Figure 5. If the overpotential is large, the Tafel equation is $\log -j = \log j_0 - (\frac{a_c n F}{2.3 RT}) \eta$ [29,30]. As seen, there are two linear regions on Pt/G and Pt/20% $\text{WO}_3\text{-G}$ catalysts, respectively. The parallel lines mean Pt/G and Pt/20% $\text{WO}_3\text{-G}$ catalysts have the similar slopes in the corresponding regions (region 1 and region 2). To be more specific, at the low current density region (region 1), the straight slopes are -69 and -63 mV/decade respectively corresponding to the oxide-covered Pt surface. Whereas, at the high current density region (region 2), the straight slopes Pt/G and Pt/20% $\text{WO}_3\text{-G}$ catalysts are -134 and -129 mV/decade respectively, an indication of an

oxide-free Pt surface. The characteristics shift in Tafel slopes suggest a change in the adsorption from the Temkin isotherm to the Langmuir isotherm [31,32]. Obviously, the shift of the slope for the Pt/20%WO₃-G catalyst occurs at around 0.70 V (vs. SCE), which is higher than that of the Pt/G catalyst (0.62 V vs. SCE). The higher potential necessary for the slope shift suggests the adsorption energy for oxygenated species is lower and the oxygenated species are easy to remove from the catalyst surface [24, 31]. Herein, oxygenated species, such as OH⁻ and O₂H⁻ on Pt surface of Pt/20%WO₃-G electrode are more weakly absorbed and easily to remove than that of Pt/G, thus, which can increase the catalytic activity for the ORR by promoting the ORR kinetics[33].

The mechanism for the improvement of catalytic activity toward oxygen reduction on the Pt/WO₃-G catalyst may be ascribed as followed:



According to Eq. (1), hydrogen tungsten bronze (H_xWO₃) was formed. And then the proton generated from Eq. (2) can be spilled over to Pt–O₂ [34], thus the oxygen reduction reaction on platinum could be catalyzed. Thus, the spillover of hydrogen between WO₃ and Pt will be facilitated by WO₃ particles. What's more, the protonation of the O₂ molecule is the rate determining step (Eq. (3)) [34,35]. Thus, the rate of oxygen reduction on the platinum gets enhanced.

So, the addition of WO₃ can probably enhance the performance of catalyst by three aspects. First, WO₃ can promote the high dispersion of the Pt nanoparticles and a narrow size distribution. Second, WO₃ can introduce the hydrogen spillover effect on Pt, which can accelerate the protonation of the O₂ molecule and the rate of oxygen reduction on the platinum. Third, the addition of WO₃ decrease the adsorption strength of oxygen containing species due to the modification of the electronic structure of Pt, which can promote the ORR kinetics, leading to an increase in the catalytic activity for the ORR.

4. CONCLUSIONS

WO₃ modified graphene fabricated by the adsorption and decomposition of ammonium metatungstate (AMT) on the surface of graphene oxide, exhibits an excellent candidate support for Pt. The Pt/WO₃-G catalysts were prepared by chemical reduction method and studied in the oxygen reduction reaction in acid media. The Pt/WO₃-G catalysts improving catalytic activity for ORR, indicates higher current densities and lower over-potential, as well as the faster reaction kinetics respect to the Pt/G catalyst. According to the XRD and TEM results, Pt/WO₃-G catalysts are composed of graphene, monoclinic WO₃ and Pt grains. And fine and uniform Pt nanoparticles are dispersed with narrower particle size distribution on Pt/WO₃-G catalysts compared to the Pt/G catalyst. Thus, the enhancement in the performance of Pt/WO₃-G catalysts is attributed to the synergistic or promotion effect of WO₃ on Pt. The interaction between Pt and WO₃ contributes to increasing the dispersion of Pt

nanoparticles, accelerating the protonation of the O₂ molecule and decreasing the adsorption strength of oxygenated species.

ACKNOWLEDGEMENTS

This work was supported by the National Natural Science Foundation of China (Nos. 21403150, 21671146, 21575097 and 21375092), Science and technology project of Zhejiang Province (Nos.2015C33224 and 2016C37040), Natural Science Foundation of Zhejiang Province, China (Nos. LQ15B060001), National Students' innovation and entrepreneurship training program (Nos. 201510350013), Zhejiang Provincial College Students' science and technology innovation project, Science and Technology Project of Taizhou City (Nos. 1202ky03).

References

1. O. Antoinea, Y. Bultel, R. Durand, *J. Electroanal. Chem*, 499 (2001) 85
2. H. Gharibi, R. A. Mirzaie, E. Shams, M. Zhiani, M. Khairmand, *J. Power Sources*, 139 (2005) 61
3. S. J. Lee, S. IIP. Yun, *Electrochim. Acta*, 52 (2007) 6525
4. H.Chhina, S. Camp bell, O. Kesler, *J. Power Sources*, 179 (2008) 50
5. T. R. Ralph, M. P. Hogarth, *Platinum Metal. Rev*, 46 (2002) 117
6. K. D. Cai, G. P. Yin, J. J. Wang, L. L. Lu, *Energy Fuels*, 23 (2009) 903
7. K. S. Novoselov, A. K. Geim, S. V. Morozov, D. Jiang, Y. zhang, S. V. Dubonos, I. V. Grigorieva, A. A. Firsov, *Science*, 306 (2004) 666
8. J. R. Williams, L. DiCarlo, C. M. Marcus. *Science*, 317 (2007) 638
9. Y. Y. Shao, S. Zhang, C. M. Wang, Z. M. Nie, J. Liu, Y. Wang, Y. H. Lin, *J. Power Sources*, 195 (2010) 4600
10. R. Kou, Y. Y. Shao, D. H. Wang, M. H. Engelhard, J. H. Kwak, J. Wang, V. V. Viswanathan, C. M. Wang, Y. H. Lin, Y. Wang, I. A. Aksay, J. Liu. *Electrochem. Commun*, 11 (2009) 954
11. Y. M. Li, L. H. Tang, J. H. Li, *Electrochem. Commun.*, 11 (2009) 846
12. O. Savadogo, P. Beck, *J. Electrochem. Soc*, 143 (1996) 3842
13. A. Lewera, L. Timperman, A. Roguska, N.A.Vante, *J. Phys. Chem. C*, 115 (2011) 20153
14. Y. Liu, S. J. Shrestha, W. E. Mustain, *ACS Catal*, 2 (2011) 456
15. M. S. Saha, Y. Zhang, M. Cai, X. L. Sun, *Int. J. Hydrogen Energy*, 37 (2012) 4633
16. X. L. Sun, M. S. Saha, M. N. Banis, Y. Zhang, R. Y. Li, X. L. Sun, M. Cai, F. T. Wagner, *J. Power. Sources*, 192 (2009) 330
17. Z. X. Yan, W. Wei, J. M. Xie, S. Meng, X. M. Lu, J. J. Zhu, *J. Power Sources*, 222 (2013) 218
18. P. Hanarp, M. Gustavsson, H. Ekstrom, L. Eurenus, G. Lindbergh, E. Olsson, B. Kasemo, *J. Power Sources*, 163 (2017) 671
19. L. Timperman, N. Alonso-Vante, *Electrocatal*, 2 (2011) 181
20. P. J. Kulesza, B. Grzybowska, M. A. Malik, M. T. Galkowski, *J. Electrochem. Soc*, 144 (1997) 1911
21. J. Shim, C. R. Lee, H. K. Lee, E. J. Cairns, *J. Power Sources*, 102 (2001) 172
22. A. K. Shukla, M. K. Ravikumar, S. Arico, G. Candiano, V. Antonucci, N. Giordano, A. Hamnett, *J. Appl. Electrochem*, 25 (1995) 528
23. Y.X. Jin, J. Zhao, F. Li, W.P. Jia, D.X. Liang, H. Chen, R.R. Li, J.J. Hu, J.M. Ni, T.Q. Wu, and D.P. Zhong, *Electrochim. Acta*, 220 (2016) 83.
24. C.A. Ma, Y.X. Jin, M.Q. Shi, Y.Q. Chu, Y.H. Xu, W.P. Jia, Q.H. Yuan, J.B.Chen, D.K. Chen, and S.M. Chen, *Journal of The Electrochemical Society*, 161 (3) (2014) F246
25. C. A. Ma, Y. Huang, Y. H. Zhu. *J. Chem. Ind. Eng.*, 60 (2009) 2633

26. L. F. Zhu, J. C. She, J. Y. Luo, S. Z. Deng, J. Chen, N. S. Xu, *J. Phys. Chem. C*, 114 (2010) 15504
27. Y. Xu, J. H. Tian, W. H. Luo, Z. Q. Shan, *J. Power Sources*, 30 (2006) 349
28. Y. Y. Shao, J. Liu, Y. Wang, Y. H. Lin, *J. Mater. Chem.*, 19 (2009) 46
29. M. Ammam, E. B. Easton. *J. Power Sources*, 236 (2013) 311
30. H. Meng , P. K. Shen. *J. Phys. Chem. B*, 109(48) (2005) 22705
31. O. Antoine, Y. Bultel, R. Durand. *J. Electroanal. Chem*, 499 (2001) 85
32. A. Damjanovic , D. B. Sepa . *Electrochim. Acta*, 35(7)(1990) 1157
33. S. J. Percival, B. Zhang, *J. Phys. Chem. C*, 117 (2013) 13928
34. B. C. Beard, J. P. Ross. *J. Electrochem. Soc*, 133(1986)1839
35. N. E. Sahin, T. W. Napporna, L. Dubauc, F. Kadirgan, J. M. Légera, K. B. Kokoha, *Applied Catalysis B: Environmental*, 203(2017) 72

© 2017 The Authors. Published by ESG (www.electrochemsci.org). This article is an open access article distributed under the terms and conditions of the Creative Commons Attribution license (<http://creativecommons.org/licenses/by/4.0/>).